

Section 2

PROGRESS IN LASER FUSION

2.A Exploding Pusher Experiments on OMEGA

Exploding pusher experiments have been conducted on the 24-beam, 10 TW OMEGA laser system. The purpose of these experiments was to activate and check out the system with targets whose behavior is relatively well understood and easily diagnosed.¹ The experimental plan also included studies of (1) the dependence of target behavior on irradiation uniformity and (2) the scaling of neutron yield with absorbed energy. Typical laser parameters were on-target energy of 500 to 800 joules and pulse width from 80 to 120 psec. Targets were 170 μm to 230 μm diameter, 0.8 μm to 1.2 μm thick glass shells filled with an equimolar mixture of DT at 20 atmospheres.²

During the program, the laser operations crew demonstrated the ability to consistently fire 24 laser beams on target once every half hour. On May 19, the highest yield efficiency (ratio of fusion energy to absorbed energy = 1.8×10^{-4}) for any laser driven target was obtained when 1.35×10^{10} neutrons were produced at a power of 7.0 TW. An additional accomplishment during this series was the successful implementation of the "knock-on" diagnostic which will be used in future high density implosion experiments to directly measure the product of density and radius, " ρR ", in the compressed DT fuel.³

Exploding Pusher Behavior⁴

In an exploding pusher shot, a short high-powered laser pulse rapidly heats a thin-wall glass microballoon (or "pusher") containing a gaseous mixture of deuterium and tritium. At the high incident intensity

($\sim 10^{15}$ W/cm²), suprathermal electrons ($\gtrsim 10$ keV in energy) are produced by the process of resonance absorption. Since the electron mean-free-path under these conditions is greater than the shell thickness, the glass is heated throughout and explodes inwardly and outwardly. The inwardly moving (or imploding) glass drives a shock wave into the DT fuel and, like a piston, does mechanical work on the fuel. High temperatures in excess of 5 keV result in the fuel and a thermonuclear burn occurs. Density in the fuel does not exceed liquid density because of premature heating of the target by suprathermal electrons and hydrodynamic shocks. (To burn a significant portion of the fuel, the DT must be compressed to over 1000 times liquid density.) The burn is quenched as the DT cools by thermal conduction to the glass and expansion.

Irradiation Uniformity

Uniformity of target irradiation or "uniformity" was varied by changing the focal point of each of the 24 lenses ($f/3.0$) with respect to the center of the target. Two extreme cases are shown in Fig. 3. Target irradiation is more uniform for "tangential focus" which corresponds to a focal point about 6 target radii ($+6R$) behind target center. All 24 beams overlap on the surface of the target and the average intensity is about 10^{15} W/cm². Irradiation is less uniform for "surface focus" for which the focus is 1 radius ($-1R$) in front of target center. The beams

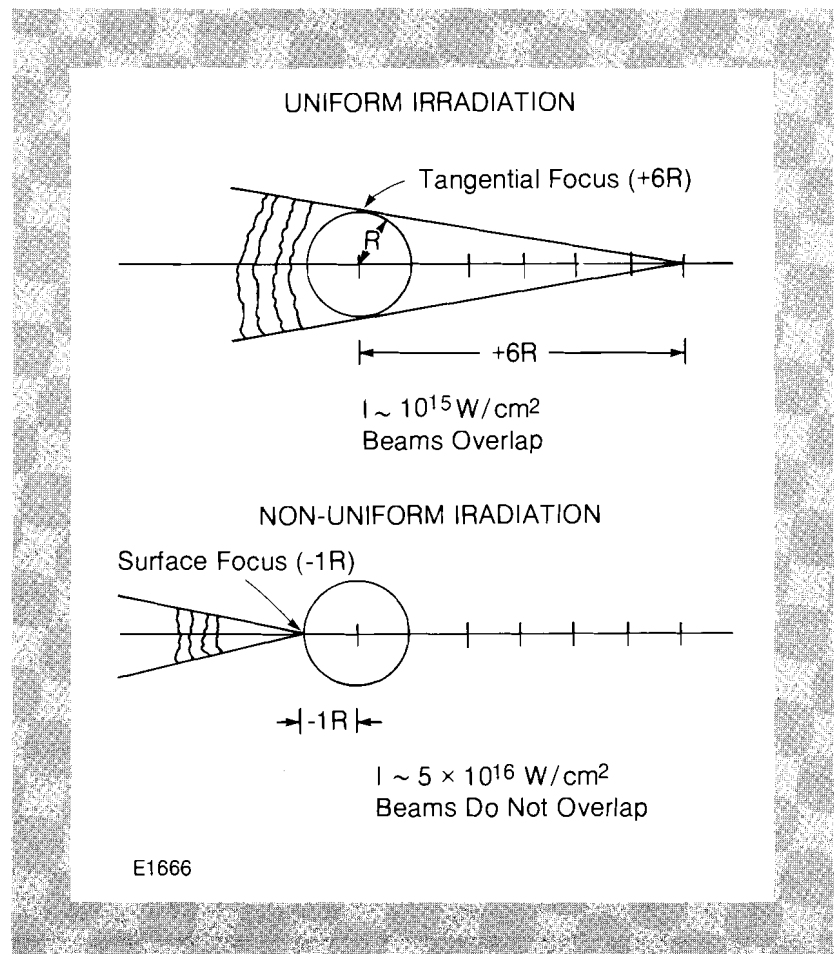


Fig. 3
Focussing geometries for most uniform
($+6R$) and least uniform ($-1R$) irradiation.

do not overlap; the energy of each beam goes into a 30 μm diameter spot in which the average intensity is about 5×10^{16} W/cm².

The sensitivity of target behavior to uniformity can be illustrated by comparing two shots which have nearly the same initial laser and target conditions but different focal positions. The initial conditions of shots 6037 and 6030 are given in Table 2. The implosion symmetries of

	Shot 6037	Shot 6030
Number of Beams	24	24
Energy on Target	694 Joules	710 Joules
Pulse Width (FWHM)	89 psec	89 psec
Power	7.8 TW	7.5 TW
Focal Position	-1 R	+4 R
Shell Diameter	207 μm	200 μm
Wall Thickness	1.0 μm	1.2 μm
DT Fill Pressure	20 atm	20 atm
Target Mass	365 ngm	389 ngm
Implosion Symmetry (see Figure 4)	Non-spherical	Nearly Spherical
Absorbed Energy	228 Joules	149 Joules
Absorption Fraction	0.33	0.21
Neutron Yield	1.01×10^{10}	3.93×10^9
LILAC Yield	3.81×10^{10}	7.97×10^9
Yield Ratio	0.27	0.49
E1741		

Table 2
Comparison of diagnostic data for shots
with different focussing.

these shots, as diagnosed with an x-ray pinhole camera, differ appreciably as shown in Fig. 4. For shot 6037 (– 1R, surface focus), there are hot and cold x-ray emission regions in the core. The structure suggests that the glass did not remain uniformly spherical as it was imploded by the 24 non-overlapping beams. For shot 6030 (+ 4R, rear focus), the near circular x-ray emission suggests that the glass retained its integrity as it imploded and stagnated against the DT fuel. The implosion symmetry is more spherical for this case in which the overlapping beams applied energy more uniformly to the surface of the pusher.

Shots 6037 and 6030 illustrate how both absorption and neutron yield change as the focal position is varied from – 1R to + 4R. As shown in Table 2, the absorption and yield for shot 6037 are 33% and 1.01×10^{10} neutrons versus 21% and 3.93×10^9 neutrons for shot

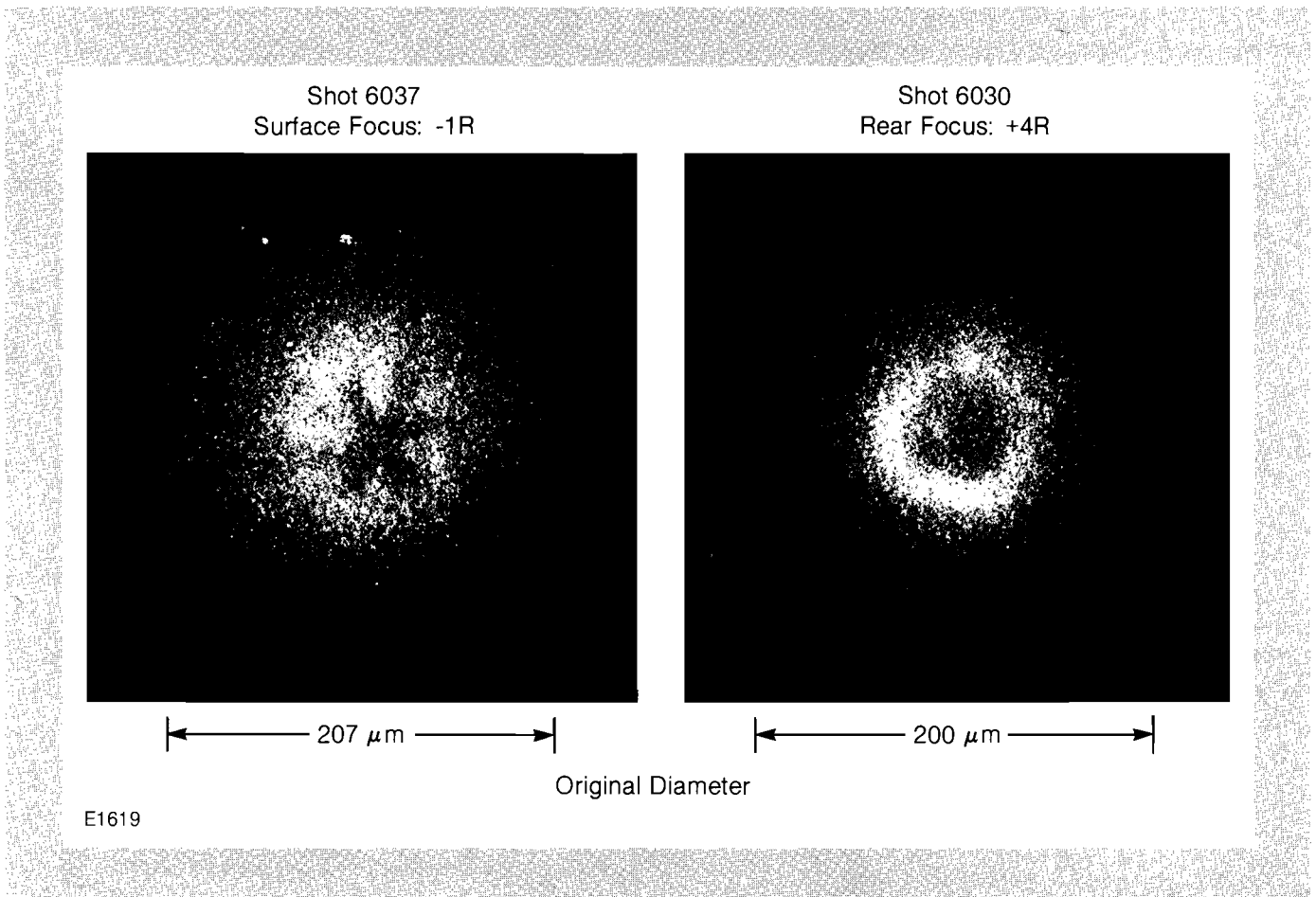


Fig. 4
Symmetry effects in 24-beam exploding
pusher shots.

6030. Results of other shots are consistent with these values. Figure 5 is a plot of absorption fraction versus focal position. Absorption varies from about 35% at surface focus to about 20% at tangential focus. For laser intensities of about 10^{16} W/cm², a resonance absorption model can be used to account for absorptions of about 20%. It is possible that the spatial modulation of the incident intensity due to non-overlapping beams and an accompanying deformation of the critical surface may explain the observed values of $\sim 35\%$ at surface focus.

Figure 6 is a plot of observed yields versus focal position for shots with incident energies between 625 and 725 joules and pulse widths between 80 and 120 psec. The higher yields at surface focus are mainly attributed to the higher absorption at that focal position.

Computer Simulations

The one-dimensional hydrodynamics code *LILAC* was used to simulate shots 6037 and 6030. The different irradiation conditions were modeled with an algorithm which estimated the on-target intensity as a function of focal position. The intensity was taken as the total laser power divided by the nominally illuminated target area. From this intensity, the suprathreshold electron temperature and the corresponding fraction of the absorbed energy lost to "fast ions" was calculated.⁵ The results are given in Table 2. As a comparison criterion, the ratio of mea-

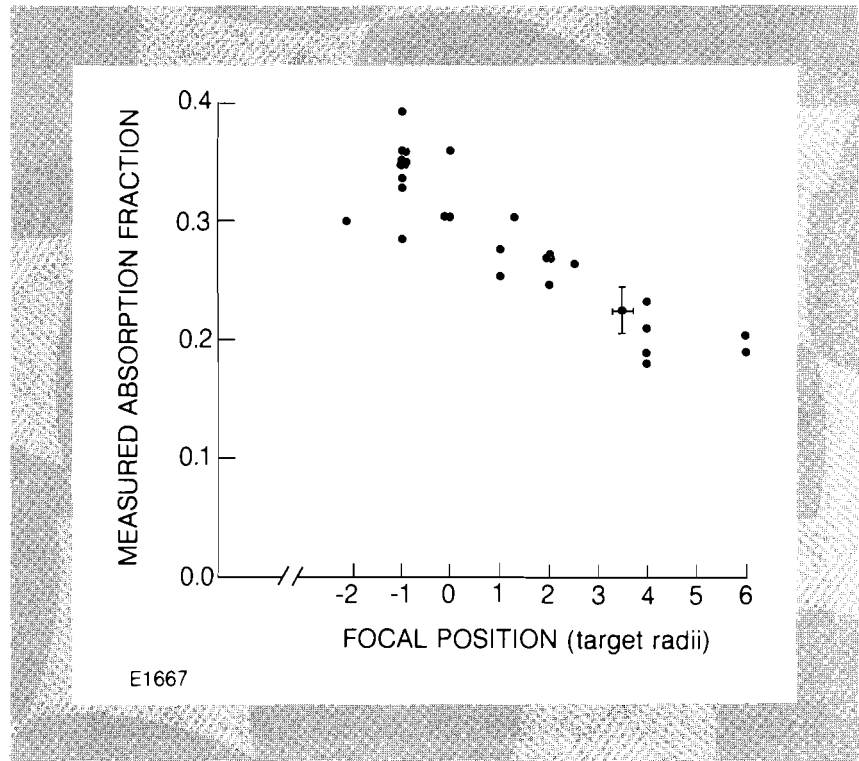


Fig. 5
Measured absorption versus focal position.

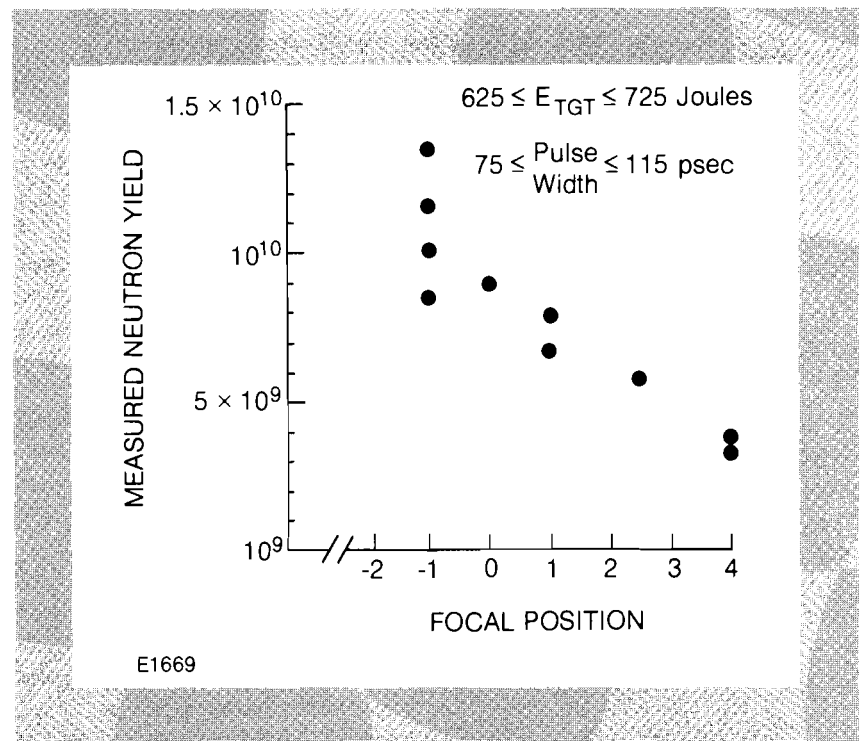


Fig. 6
Measured neutron yield versus focal position.

sured to simulated neutron yield is used. For the shot at $-1R$, this yield ratio is 0.27; for the shot at $+4R$, the ratio is 0.49. The better relative agreement of shot 6030 with simulation is attributed to its more uniform irradiation which led to a more spherical implosion symmetry. This symmetry is in better agreement with the assumption of one-dimensionality which underlies the code calculation.

It is interesting to note that target performance is only a factor of 2 higher for the uniform ($+4R$) shot than for the non-uniform shot ($-1R$). This is an attribute of fast electron driven implosions in which energy smoothing due to the large fast electron range tends to reduce sensitivity to irradiation uniformity.

Neutron Yield Scaling

The observed dependence of neutron yield on specific absorbed energy, ϵ_A , is shown in Fig. 7. The reason for plotting the data against ϵ_A (absorbed energy divided by target mass) is that alpha particle and neutron time of flight spectra indicate that the DT ion temperature, θ_i , scales almost linearly with ϵ_A^6 ; an approximate ($\pm 30\%$) relation is $\theta_i \approx 10 \epsilon_A$ where ϵ_A is in joules per nanogram and θ_i is in keV. The yields acquired for $+1R$ to $+4R$ focusing are consistent with a curve of simulated *LILAC* yields scaled by a factor of 2. The *LILAC* simulations

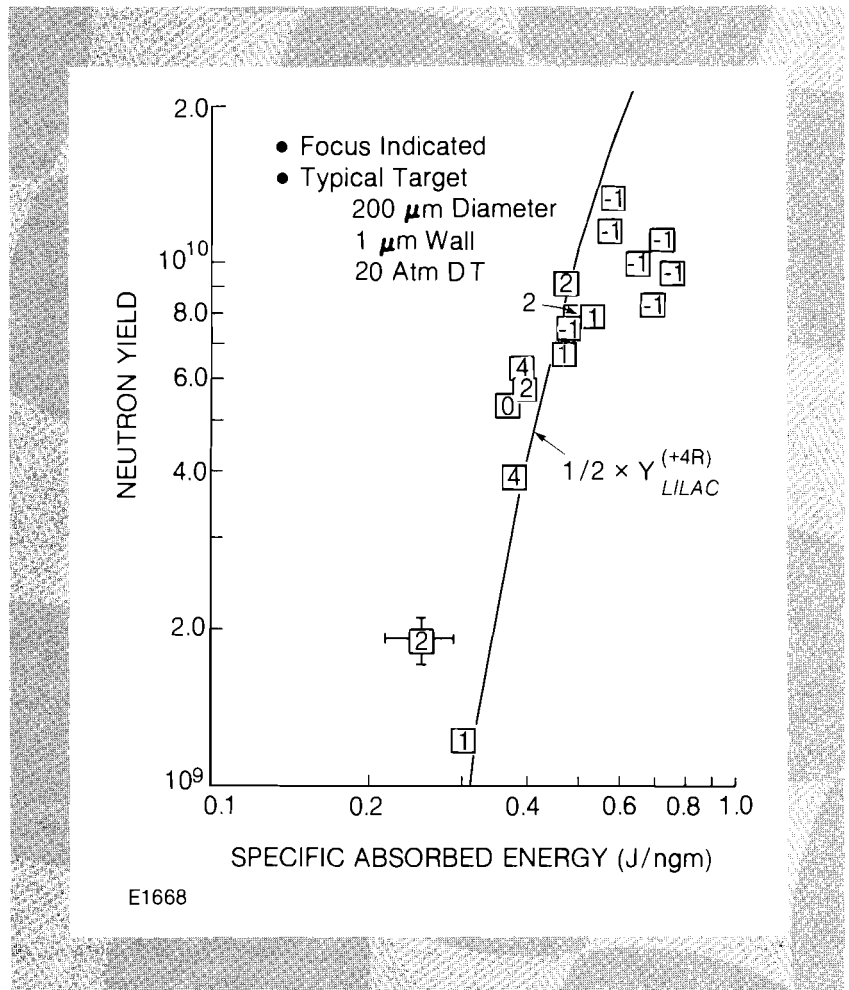


Fig. 7
 Measured neutron yield versus specific absorbed energy.

were done for a focus of $+4R$ and a typical target of $200\ \mu\text{m}$ diameter, $1\ \mu\text{m}$ wall, and a 20 atmosphere DT fill. At $\epsilon_A = 0.5\ \text{J/ng}$, the curve of simulated yields scales as $Y_{LILAC} \sim \epsilon_A^{3.9}$. This scaling is primarily due to the ion temperature dependence⁷ of the Maxwell velocity-averaged DT cross section $\langle \sigma v \rangle$ which, at an equivalent temperature $\theta_i = 5\ \text{keV}$, varies as $\theta_i^{3.2}$. The relative normalization between the data and code is, in part, dependent on the code's simulation of focusing conditions which affects both the implosion symmetry and the partition of absorbed laser energy between fast ions and the implosion.

Fuel ρR

The Lawson Criterion for scientific breakeven is expressed as a requirement that the product, " ρR ," of the density and radius in the compressed fuel be greater than $\sim 0.3\ \text{gm/cm}^2$ for an ion temperature of about 5 keV. A method—called the "knock-on" diagnostic—has been developed to directly measure the fuel ρR . Track detectors⁸ made from CR-39 are used to count the deuterium and tritium ions elastically scattered out of the fuel by 14 MeV neutrons. The observed number of D and T ions is proportional to the average fuel ρR at peak burn.

The feasibility of the knock-on diagnostic has been demonstrated by measuring (simultaneously) various portions of the velocity-squared (or E/A, kinetic energy per nucleon) spectrum of the D and T ions. A different thickness tantalum foil was used to slow and shift each part of the spectrum into an E/A range where both track registration and background discrimination can be achieved with the CR-39. To separate knock-on particles (deuterons and tritons) from the dominant background due to protons, track criteria based on velocity and range are used. Track diameter is used to determine particle velocity. A minimum particle range is established by requiring a spatially coincident pair of track diameters from the particle's entering and exiting the $150\ \mu\text{m}$ thick CR-39.

Four spectral regions probed with different detector-foil combinations (tantalum thicknesses $50\ \mu\text{m}$, $75\ \mu\text{m}$, $95\ \mu\text{m}$, and $115\ \mu\text{m}$) are shown in Fig. 8; a fifth combination ($160\ \mu\text{m}$ thick) was used to make a null measurement by stopping all knock-on particles. Tracks were obtained from an integrated exposure to two similar OMEGA shots (shots 6037 and 6038). The bar graph at the bottom shows that the measured (shaded) and expected fractions of the total signal are consistent for each region of the E/A spectrum. This consistency demonstrates the feasibility of using track detectors to probe the knock-on spectrum. Moreover, this same data can be used to determine the average ρR for the two shots. The result is $\rho R \sim 1.5 \times 10^{-4}\ \text{gm/cm}^2$ which is within 30% of the value predicted by *L/LAC* simulation.

Summary

The OMEGA laser system has been activated for 24-beam implosion experiments at a wavelength of $1.054\ \mu\text{m}$. Good reproducibility has been demonstrated in the control of laser parameters such as total energy, beam balance, and pulse shape. The effect of irradiation uniformity on implosion symmetry, absorption fraction, and neutron yield has been studied. The neutron yields measured in initial exploding pusher experiments are reasonably consistent with expectations

based on *LILAC* computer simulations. In addition to the usual diagnostics for energy balance, x-ray imaging, and fusion yield, a new technique has been developed to directly measure the ρR of the compressed fuel.

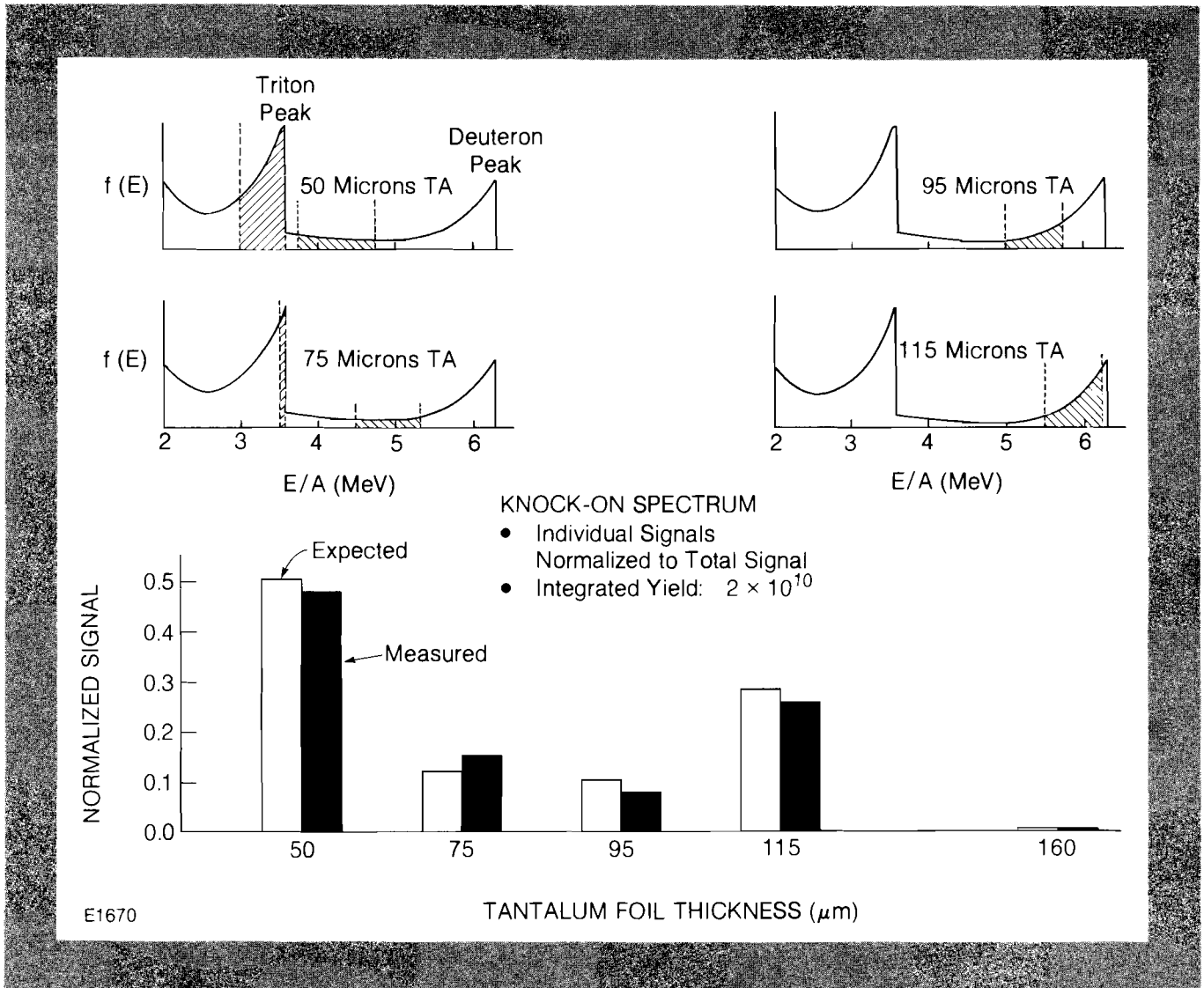


Fig. 8
Measurement of different intervals of the "knock-on" spectrum.

REFERENCES

1. J. M. Soures et al., "A Review of High Density, Laser Driven, Implosion Experiments at the Laboratory for Laser Energetics," *Laser Interaction and Related Plasma Phenomena*, vol. **5**, edited by H. J. Schwarz, H. Hora, M. Lubin and B. Yaakobi (Plenum Publishing Corp., 1981); B. Yaakobi et al., *Phys. Rev. A* **19**, 1247 (1979); E. K. Storm et al., *Phys. Rev. Lett.* **40** (1978); H. G. Ahlstrom, *Appl. Opt.* **20**, 1902 (1981).
2. Some of these targets were produced by KMS Fusion, Ann Arbor, Michigan.
3. S. Skupsky and S. Kacenjjar, *J. Appl. Phys.* **52**, 2608 (1981).

4. E. Storm, *Laser Program Annual Report - 1977*, Lawrence Livermore National Laboratory, **UCRL-50021-77** (1978), pp. 6-38; M. Rosen and J. Nuckolls, *Phys. Fluids* **22**, 1393 (1979).
5. K. Estabrook and W. L. Kruer, *Phys. Rev. Lett.* **40**, 42 (1978).
6. For neutron time of flight data, see Fig. 5-55, *Laser Program Annual Report - 1978*, Lawrence Livermore National Laboratory, Livermore, Calif., **UCRL-50021-78**, p. 5-44; for alpha time of flight data, see session 5R3, *Bulletin of the American Physical Society* **25**, 931 (1980).
7. E. J. Stoval, unpublished; cited in S. Glasstone and R. H. Lovberg, *Controlled Thermonuclear Reactions* (Van Nostrand, Princeton, 1960), p. 20.
8. S. P. Ahlen, P. B. Price and G. Tarle, *Physics Today* **34**, 32 (1981).